Electronic Supplementary Material (ESI) for Energy & Environmental Science.
This journal is © The Royal Society of Chemistry 2023

Supporting Information

Synergistic Effect of Dry Air and Surfactants Enables Water a Promising Green Solvent for Stable and Efficient Perovskite Solar Cells

Yanrui Zhang[1#], Lixia Ren[1#], Peng Zhai[1*], Jingjing Xin[1], Jiarong Wu[1], Qi Zhang[1], Xin Chen[1], Kui Zhao[1], Lu Zhang[1], Shengzhong (Frank) Liu[1,2,*]

[1]Key Laboratory for Applied Surface and Colloid Chemistry, National Ministry of Education; Shaanxi Engineering Lab for Advanced Energy Technology; School of Materials Science and Engineering, Shaanxi Normal University, Xi'an 710119, China.
[2]Dalian Institute of Chemical Physics, Chinese Academy of Sciences, Dalian, 116023, China; Center of Materials Science and Optoelectronics Engineering, University of Chinese Academy of Sciences, Beijing 100049, P. R. China.

[#] These authors contributed equally in this work.

[*] Correspondence: zhaipeng@snnu.edu.cn; szliu@dicp.ac.cn

Experimental section

Materials

$Pb(NO_3)_2$ (> 99%) and $C_{18}H_{33}KO_2$ (> 99%) were purchased from Sigma-Aldrich. Formamidinium iodide (FAI), methylammonium iodide (MAI), methylammonium chloride (MACl) and *n*-octylammonium iodide (OAI) were purchased from Xi'an Polymer Light Technology Corp.

Device fabrication

Fluoride-doped tin oxide glass substrate was sequentially cleaned by 2% commercial detergent water solution, deionized water, ethanol and acetone in ultrasonic bath for 15 min, rinsed with deionized water and then dried by air blowgun. After O_3/ultraviolet treatment for 15 min, the 40 nm compact layer TiO_2 (c-TiO_2) was deposited on a cleaned FTO substrate by chemical bath method. The mesoporous TiO_2 (mp-TiO_2) was spin-coated at 4000 rpm for 20 s onto the c-TiO_2 using a commercial paste (Greatcell 30 NR-D) diluted in ethanol (1:6, weight ratio) to achieve 150 to 200 nm thickness. After drying at 80 °C for 10 min, the TiO_2 films were gradually sintered to 500 °C, kept at this temperature for 30 min and cooled to room temperature. Before use, the films were treated with Li_2CO_3 aqueous solution (1 mg/mL) by spin coating at 3000 rpm for 20 s and then were sintered at 450 °C for 30 min. After cooling down to room temperature and O_3/ultraviolet treatment for 15 min, the substrates were transferred to dry-air glovebox (relative humidity < 10%) for deposition of perovskite films. Pristine aqueous $Pb(NO_3)_2$ solution (1.5 M) was prepared by adding $Pb(NO_3)_2$ into DI water, followed by sonicating for 1 hour to form the stable solution. Note that when PO is added to $Pb(NO_3)_2$ aqueous solution, oleate ions will first react with Pb^{2+} and form precipitation. After stirring for a while, the precipitate will dissolve in the ink and form a stable solution. To reduce the consumption of toxic Pb, dynamic spin coating method was employed. During the high-speed spin coating process, the intense friction between the substrate and air would cause TiO_2 meso-layer to adsorb a large amount of water vapor. $Pb(NO_3)_2$ solution was spin coated onto the substrate at 5000 rpm for 20 s, and dried at 80 °C on

a hot plate for 30 min. After cooling to room temperature, the $Pb(NO_3)_2$-infiltrated mesoporous TiO_2 film was immersed in an IPA solution containing MAX (MAI/MACl = 4:1) with the concentration of around 12 mg/mL. The total incubation time was split into 3 sectors. For instance, the total dipping time was 10 min, in which the first cycle lasted 4 min and the other two cycles needed 3 min for each. After the conversion of $Pb(NO_3)_2$ to $MAPbI_{3-x}Cl_x$ is completed, a solution of FAI: MAI: MACl (25mg: 2.5mg: 2.5mg in 1ml IPA) was spin-coated atop the $MAPbI_{3-x}Cl_x$ layer at a spin rate of 2000 rpm for 30 s, followed by annealing at 150 °C for 10 min to obtain FA-rich perovskite film. Upon cooling to room temperature, OAI solution (4 mg/mL in IPA) was spin coated on the perovskite at 5000 rpm for 30 s, followed by 100 °C for 10 min. The hole-transport layer precursor was prepared by dissolving 72.3 mg spiro-OMeTAD, 28 μL 4-tert-butylpyridineand 17.5 μL bis(trifluoromethane) sulfonimide lithium salt solution (520 mg Li-TFSI in 1 mL acetonitrile) in 1 mL chlorobenzene. The precursor was then spin-coated on the perovskite layer at 4000 rpm for 30 s. The solar cells were then transferred to a box with dry air (humidity lower than 20% RH) for oxidation for 16 h. Finally, a 80-nm-thick metal electrode was thermally evaporated onto the stack.

Thin films characterizations

Surface morphology images of the perovskite films or PSC devices were obtained using a field emission scanning electron microscope (Jeol SU-8020). X-ray diffraction (XRD) patterns were acquired using a Bruker D8 GADDS diffractometer with the Cu Kα radiation. The XPS measurements were performed in a VG ESCALAB MK2 system with monochromatized Al Kα radiation at a pressure of 5.0×10^{-7} Pa. The absorption spectra of the annealed perovskite films were obtained by a Shimadzu UV-3600 spectrophotometer. Topography and YM maps were acquired using a Bruker Dimension ICON with one advanced PeakForce-QNM mode and the probe tip with a force constant of about 200 N/m and a curvature radius of about 20 nm, which can detect nanoscale heterogeneity. Time-of-flight secondary ion mass spectrometry (ToF-SIMS) depth analysis was performed on a TOF-SIMS 5-100 spectrometer (ION-

TOF GmbH) using GCIB as sputter source. Carrier lifetime fluorescence spectra were measured by fluorescence lifetime imaging microscopy (FLIM) (PicoQuant,Micro Time200). The TAS measurements were performed at 14.90 μJ/cm^2. The femtosecond laser pulse was generated by a Ti:sapphire femtosecond regenerative amplifier with 500 nm wavelength and 50 kHz repetition rate (Coherence) and served as both pump and probe beams. The spot size of the TA is approximately 0.008 mm^2 as evaluated by imaging the laser spot. All experiments were carried out at room temperature (i.e.,T= 300 K).

Device measurements

Before measurement, a non-reflective metal mask with aperture area (0.09 cm^2) was covered on the top of the device (0.10 cm^2) to precisely define the active area and ensure that no illumination or voltage biasing condition had been introduced. The current-voltage (IV) scan was recorded with a computer-controlled digital source meter (Keithley 2400) under exposure of a solar simulator (XES-40S2-CE, Class AAA, San-Ei Electric, AM 1.5G filter at 100 mW cm^{-2}). The light intensity of 1 Sun illumination was calibrated using a Si-reference cell (the 91150V model, Newport, UK). The voltage scan rate was 50 mV s^{-1} in forward and reverse scans under ambient conditions (25 ºC, relative humidity ~ 40%). EQE spectra of PSCs were measured using a Q Test Station 500TI system (Crowntech, Inc. USA). The monochromatic light intensity was adjusted using a reference silicon detector. In the light intensity dependent V_{OC} examination, the light intensity was controlled using an ND filter (Shibuya Optical Co., LTD, Japan) that covered the top of the device. All photovoltaic parameters were extracted from the average IV curve of forward (from short-circuit to open-circuit) and reverse (from open-circuit to short-circuit) scans. For the operational stability test, the unencapsulated PSC devices were measured through MPP tracking under continuous 1 sun-equivalent illumination in a N_2-filled glove box with a temperature of 30 °C (100 mW/cm^2, white LED).

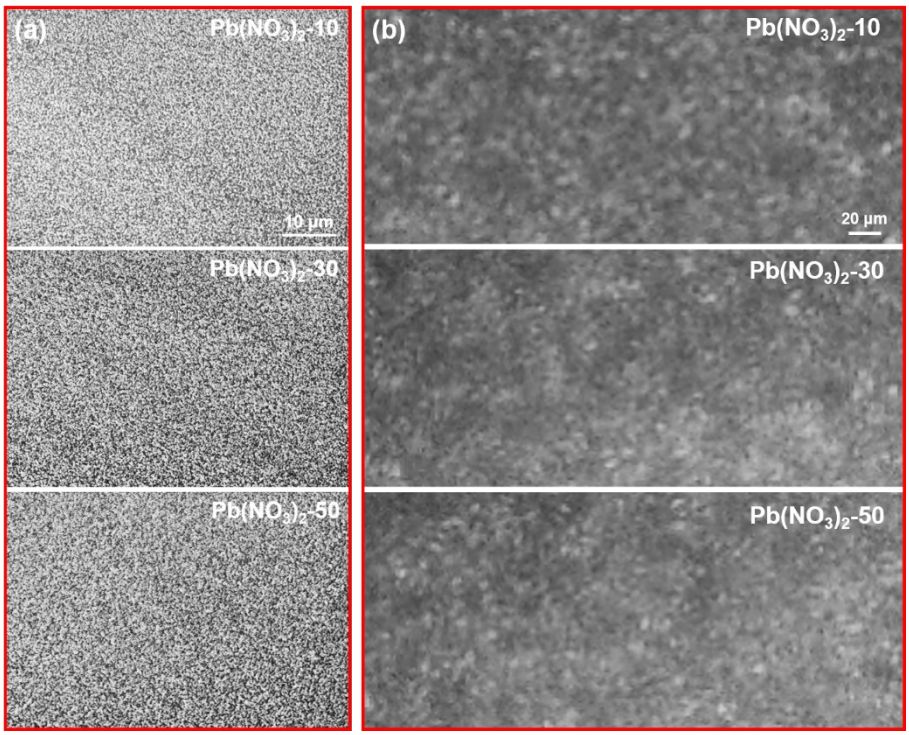

Figure S1. a) SEM and b) OM images of $Pb(NO_3)_2$ films deposited under different humidity conditions.

Under dry air conditions, a large-area thin film with increased coverage can be obtained, while samples prepared under humid air conditions reveal numerous voids (black area). OM image shows that the grain boundaries in the $Pb(NO_3)_2$-10 film merge together, thereby reducing the number of voids.

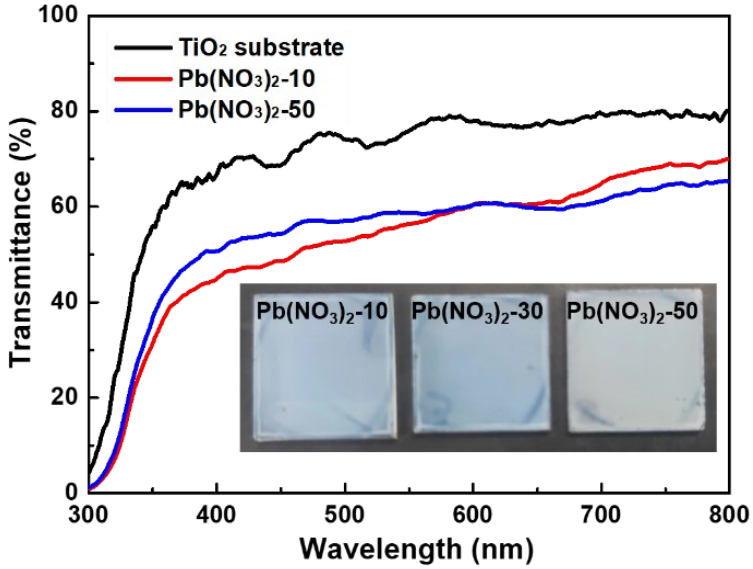

Figure S2. The UV-vis transmittance of TiO_2 substrate and $Pb(NO_3)_2$ substrates.

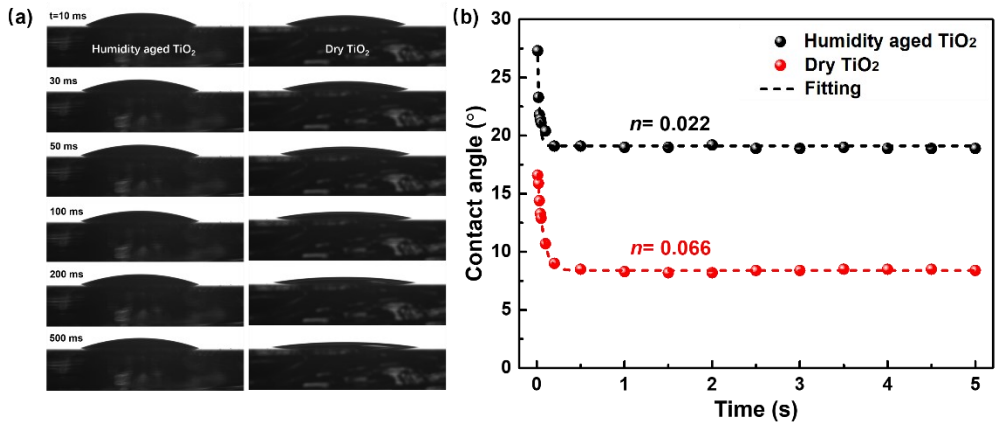

Figure S3. a) Dynamics of liquid spreading on various TiO_2 substrates. Selected images showing the spreading of PEDOT-PSS droplet at the early stages after contacting with a humidity-aged TiO_2 and a dry TiO_2 surface. The static contact angles for the TiO_2 and the surfaces are 18.9° and 8.5°, respectively. b) Contact angle variation as a function of time for various TiO_2 substrates.

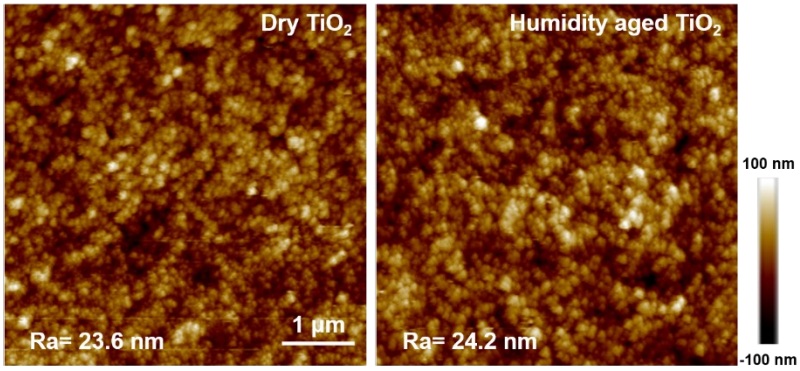

Figure S4. AFM topographic image of dry and humidity aged TiO_2 substrates.

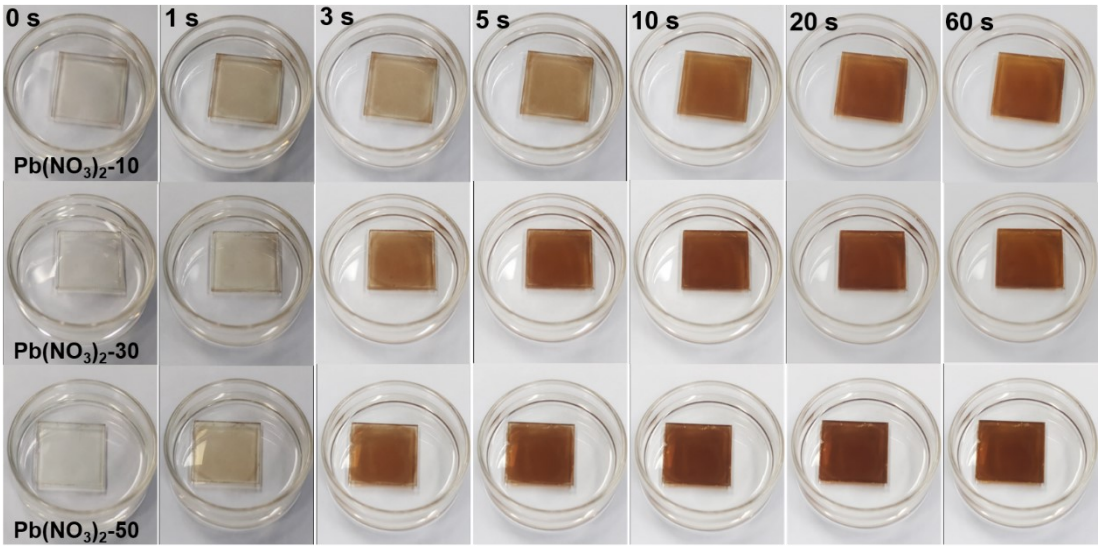

Figure S5. Snapshots of the dynamic conversion process from $Pb(NO_3)_2$ to perovskite.

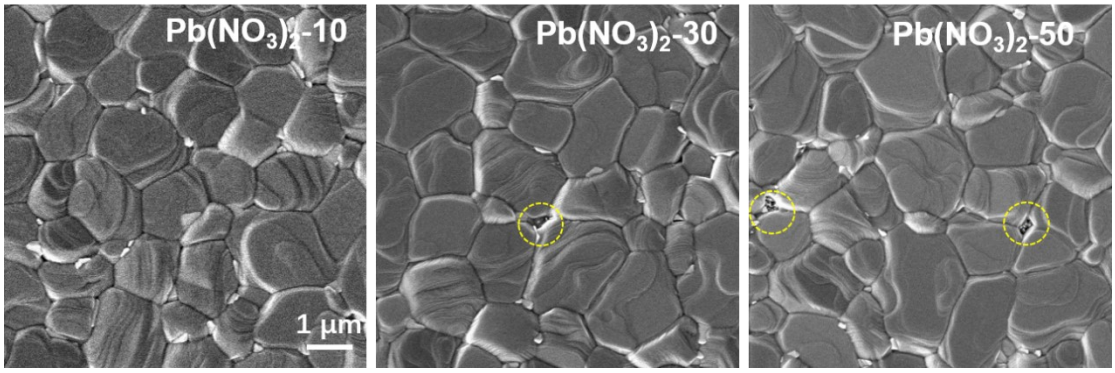

Figure S6. SEM images of perovskites prepared from various $Pb(NO_3)_2$ films. The yellow circle refers to the pinhole defects present in the surface.

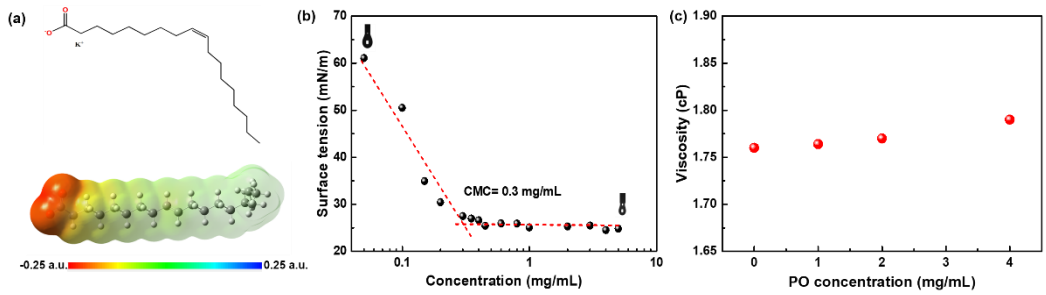

Figure S7. a) The ESP map of PO without cation ion. The corresponding maximum and minimum values of ESP are provided below the map. b) Surface tension as a function of PO concentration. c) Viscosities of the solutions measured with a rotary viscosimeter at the shear rate 150 s^{-1}.

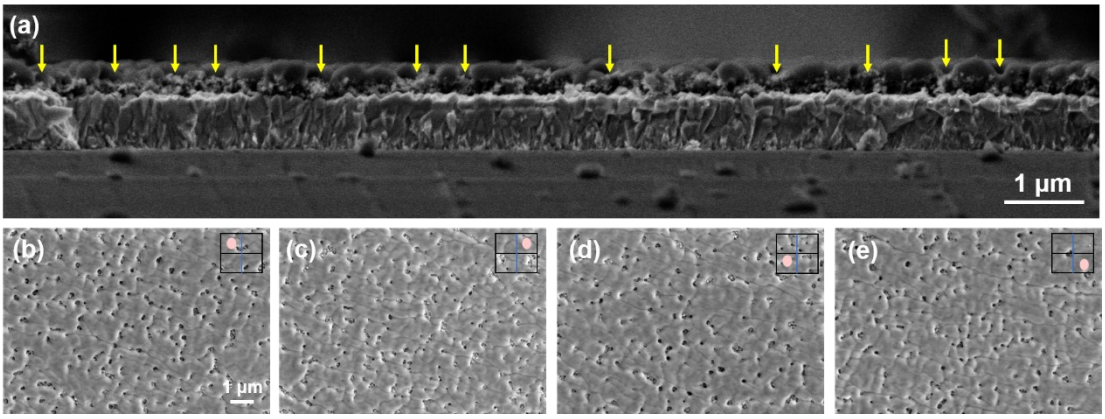

Figure S8. a) Cross-sectional image of $Pb(NO_3)_2$ film. The yellow arrow refers to the micro-voids. b-e) SEM images of different parts of $Pb(NO_3)_2$ film.

Figure S9. The static contact angle (θ< 5º) between the TiO_2 substrate and the water with PO-2mg

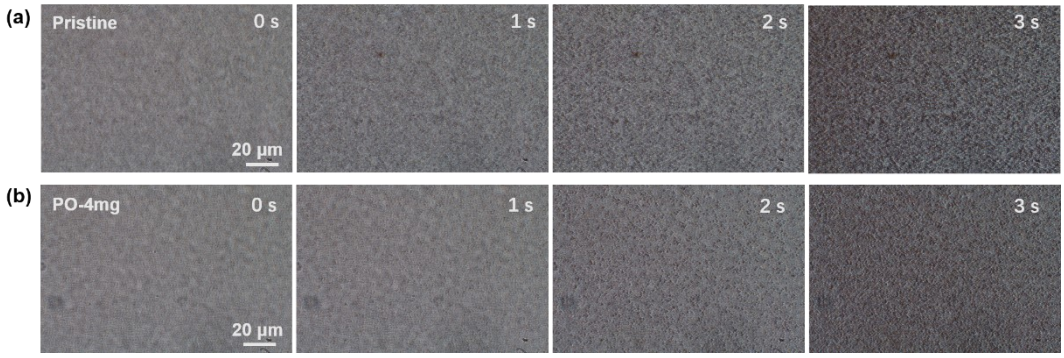

Figure S10. Optical images of the real-time perovskite crystallization. a) the pristine $Pb(NO_3)_2$ and b) PO-4mg treated $Pb(NO_3)_2$.

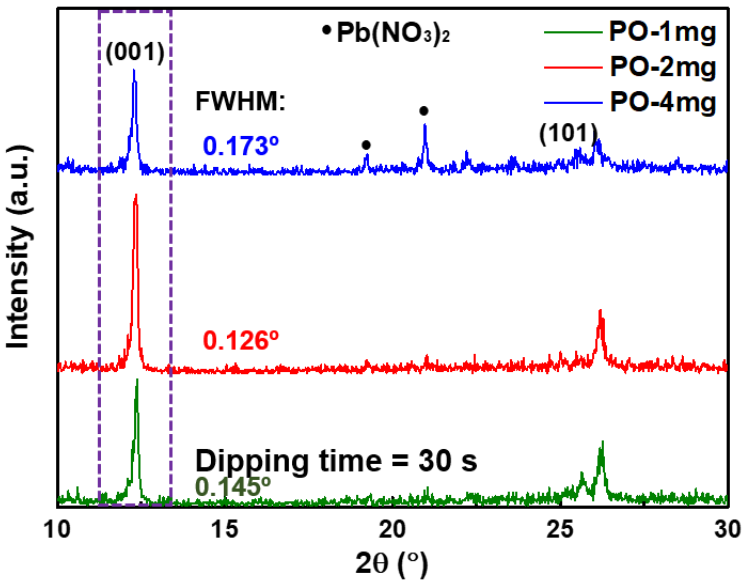

Figure S11. XRD spectra of the intermediate PbI_2 converted from the various $Pb(NO_3)_2$.

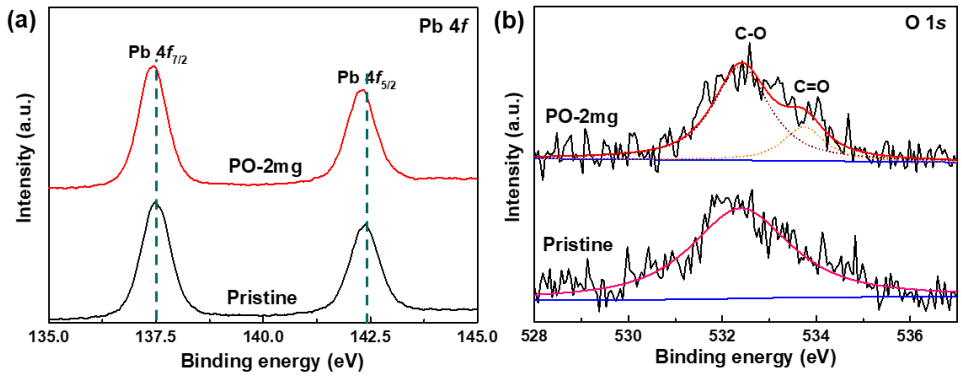

Figure S12. XPS spectra of perovskite films prepared from pristine $Pb(NO_3)_2$ and PO treated $Pb(NO_3)_2$, narrow scanning XPS spectra of a) Pb 4*f* and b) O 1*s*.

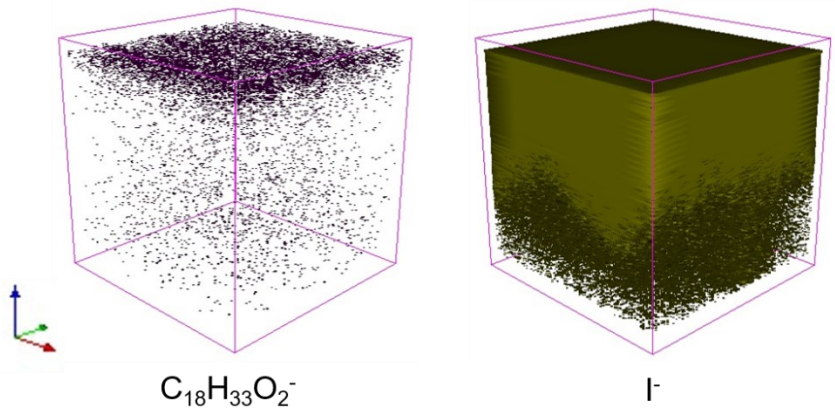

Figure S13. ToF-SIMS depth profiles. The tracked ions are all negatively charged monovalent fragments and the tracked m/z values are 281 ($C_{18}H_{33}O_2^-$) for oleate and 127 (I^-) for I.

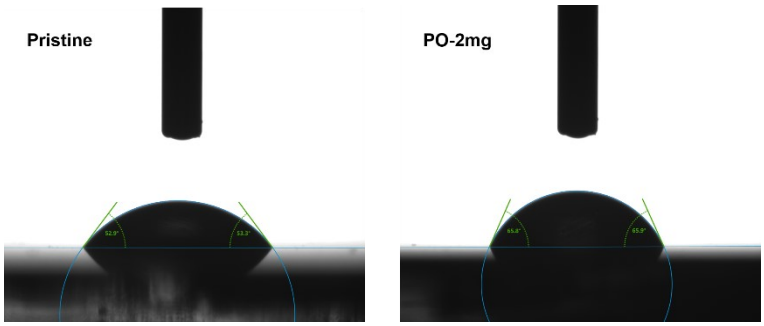

Figure S14. Contact angle of pristine and PO treated perovskites.

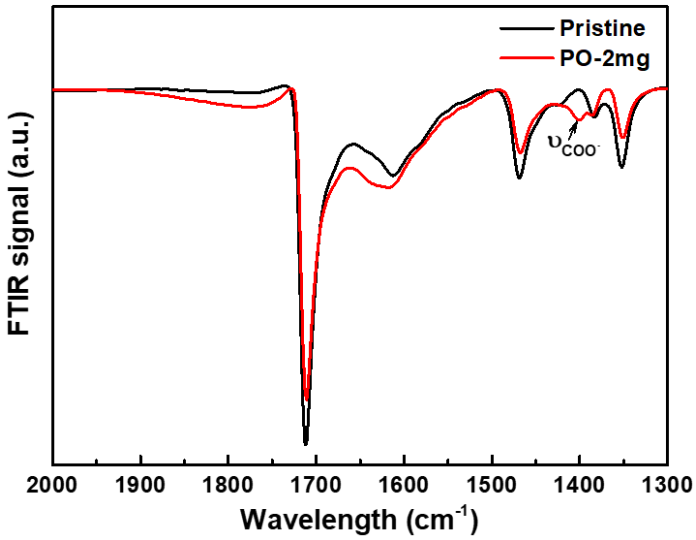

Figure S15. FTIR spectra of pristine and PO treated perovskites.

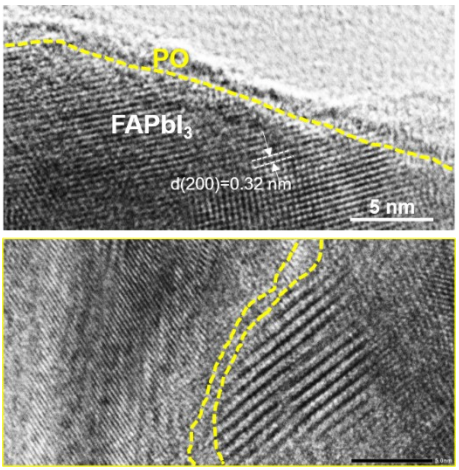

Figure S16. HRTEM micrograph for PO treated perovskite film.

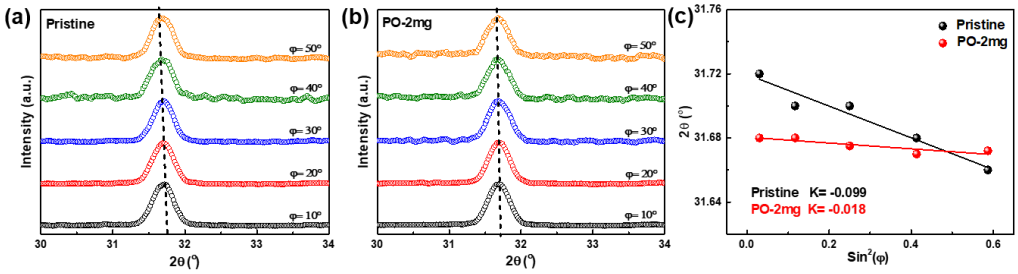

Figure S17. Residual strain distribution measurement of (a) the pristine and (b) PO treated perovskite films. (c) Liner fitting of 2θ-$\sin^2(\psi)$ derived from the GIXRD patterns with various ψ values.

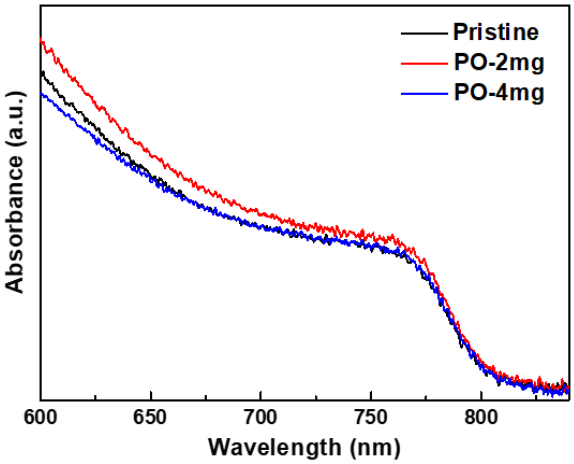

Figure S18. UV-Vis absorbance of pristine and PO treated perovskites.

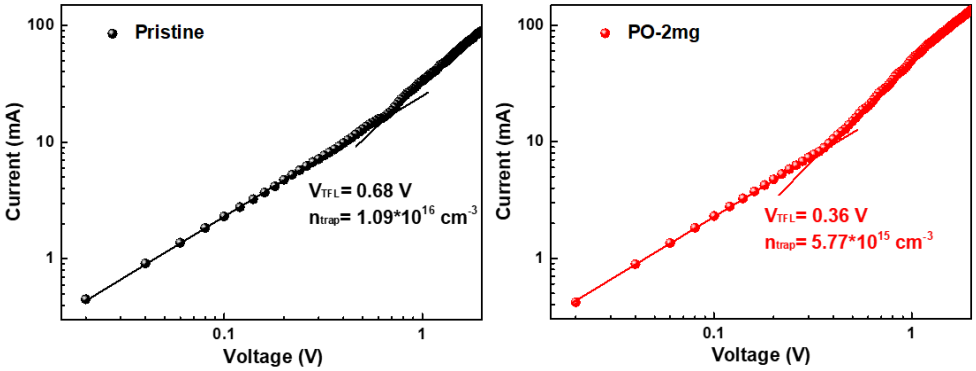

Figure S19. Space-charge-limited current (SCLC) measurements with an electron-only FTO/c-TiO_2/mpTiO_2/perovskite/PCBM/Ag structure

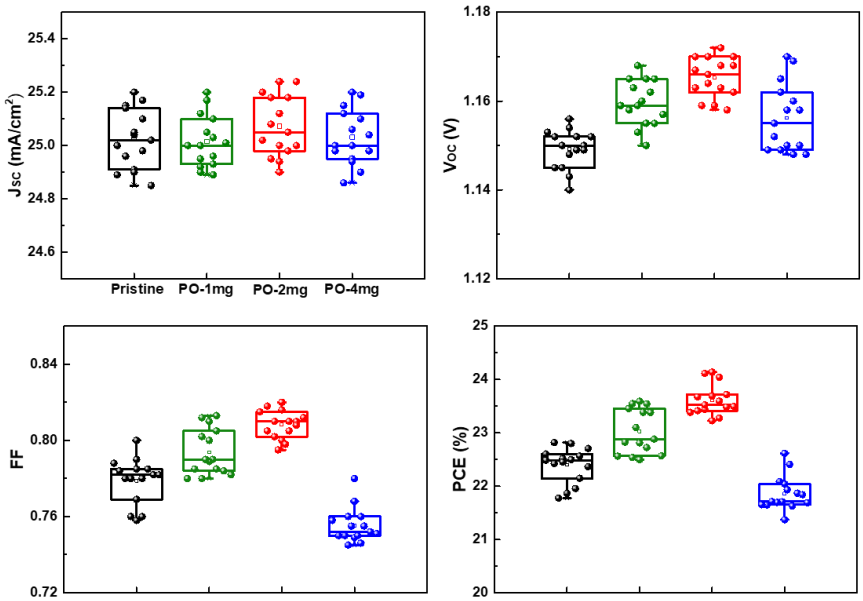

Figure S20. Statistical distribution diagram of the devices. Box plots of I-V characteristics of PSCs made with different perovskite.

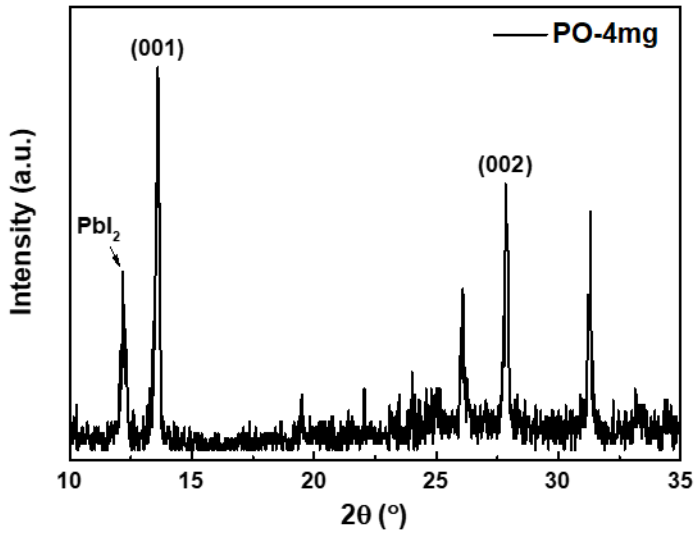

Figure S21. XRD spectra of the perovskite treated with PO-4mg.

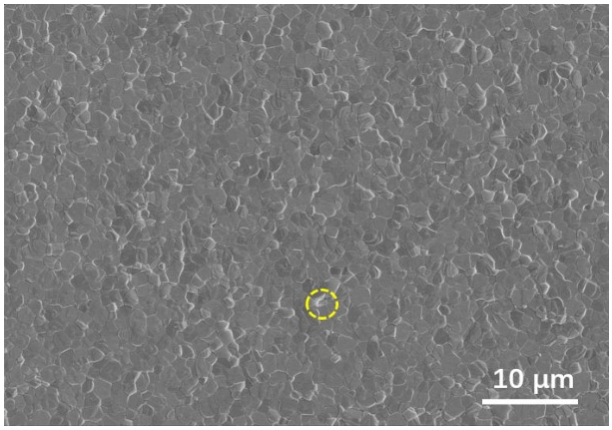

Figure S22. SEM image of pristine perovskite on a large area. The yellow circle refers to the pinhole defects present in the surface.

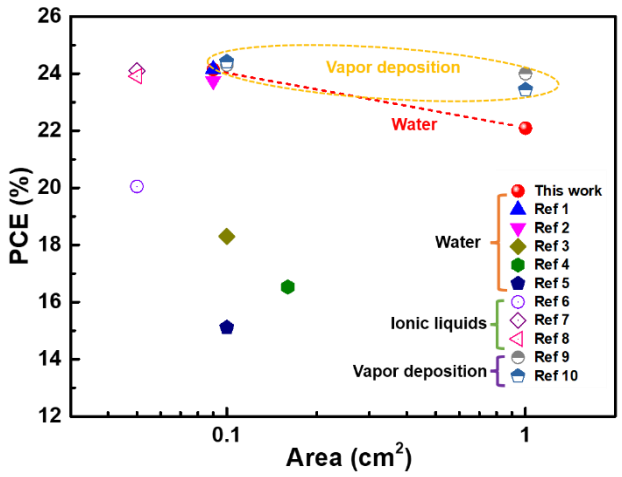

Figure S23. Performance comparison between various green fabrication methods.[1-10]

The state-of-the-art green methods for preparing perovskite include vapor deposition (vacuum evaporation) and green solvent deposition (ionic liquids, water). It is recognized that the perovskite film prepared by vapor deposition maintains excellent uniformity and consistency on a large area scale. However, it requires relatively high production costs and is limited by chamber size. Perovskites prepared from water and ionic liquids (methylamine formate, methylammonium acetate) have been confirmed to be highly preferred and promising. Based on the $Pb(NO_3)_2/H_2O$ protocol, we have developed an ecofriendly scheme to address the issue of waste lead recycling and disposal, aiming to prevent the harm of Pb^{2+} to human health. However, fabrication using ionic liquids cannot recycle waste lead and solvents, which will increase the production cost. In conclusion, even though the PCE of large area (1 cm^2) devices prepared by water is slightly lower than that of devices prepared by vacuum evaporation, it has significant advantages in terms of low carbon emissions and low cost of the entire process.

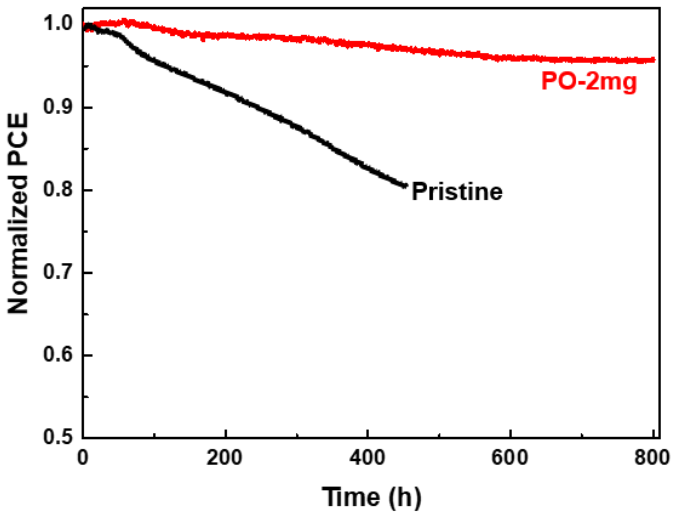

Figure S24. Normalized power output of PSCs at maximum power point (MPP) under one sun equivalent illumination.

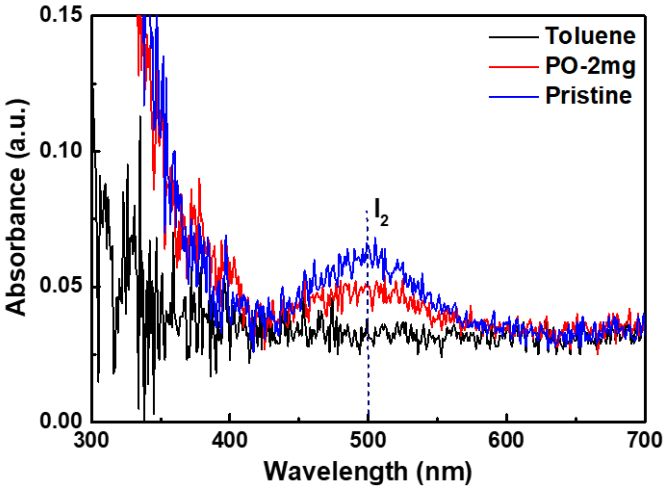

Figure S25. UV-vis absorptions recorded for the toluene taken from the pristine and PO-treated perovskites at 24 hours aging time.

Table S1. Total free surface energy (γ_s), and its dispersive (γ_s^d) and polar (γ_s^p) components calculated using the Owens-Wendt model.

Substrate	γ_s (mJ·m^{-2})	γ_s^d (mJ·m^{-2})	γ_s^p (mJ·m^{-2})
Dry TiO_2	291.83	112.08	179.75
Humidity aged TiO_2	69.50	28.53	40.97

Table S2. Photovoltaic parameter deviation of the PSCs prepared from pristine and PO treated films.

Device	V_{OC} (V)	J_{SC} (mA cm^{-2})	FF (%)	PCE (%)
Pristine	1.149 ± 0.004	25.02 ± 0.111	77.89 ± 0.012	22.40 ± 0.324
PO-1mg	1.160 ± 0.005	25.02 ± 0.109	79.38 ± 0.012	23.03 ± 0.404
PO-2mg	1.165 ± 0.005	25.07 ± 0.114	80.83± 0.007	23.61 ± 0.288
PO-4mg	1.156 ± 0.008	25.03 ± 0.104	75.53 ± 0.009	21.86 ± 0.321

Reference

1. P. Zhai, L. Ren, Y. Zhang, Z. Xu, Y. Wu, K. Zhao, L. Zhang and S. Liu, *Energ. Environ. Sci.*, 2023, **16**, 3014-3024.
2. P. Zhai, L. Ren, S. Li, L. Zhang, D. Li and S. Liu, *Matter*, 2022, **5**, 4450-4466.
3. T. Y. Hsieh, M. Pylnev, E. Palomares and T. C. Wei, *Adv. Funct. Mater.*, 2020, **30**, 1909644.
4. B. Zhang, Y. Xiao, Y. Liu, X. Yu, Z. Ku, W. Li, J. Xiao, F. Long, Y. Cheng and Y. Peng, *ACS Sustainable Chem. Eng.* , 2022, **10**, 5225-5232.
5. T.-Y. Hsieh, T.-S. Su, M. Ikegami, T.-C. Wei and T. Miyasaka, *Mater. Today Energ.*, 2019, **14**, 100125.
6. L. Chao, Y. Xia, B. Li, G. Xing, Y. Chen and W. Huang, *Chem*, 2019, **5**, 995-1006.
7. W. Hui, L. Chao, H. Lu, F. Xia, Q. Wei, Z. Su, T. Niu, L. Tao, B. Du, D. Li, Y. Wang, H. Dong, S. Zuo, B. Li, W. Shi, X. Ran, P. Li, H. Zhang, Z. Wu, C. Ran, L. Song, G. Xing, X. Gao, J. Zhang, Y. Xia, Y. Chen and W. Huang, *Science*, 2021, **371**, 1359–1364.
8. L. Chao, Y. Xia, X. Duan, Y. Wang, C. Ran, T. Niu, L. Gu, D. Li, J. Hu, X. Gao, J. Zhang and Y. Chen, *Joule*, 2022, **6**, 2203-2217.
9. L. Tan, J. Zhou, X. Zhao, S. Wang, M. Li, C. Jiang, H. Li, Y. Zhang, Y. Ye, W. Tress, L. Ding, M. Gratzel and C. Yi, *Adv. Mater.*, 2023, **35**, e2205027.
10. H. Li, J. Zhou, L. Tan, M. Li, C. Jiang, S. Wang, X. Zhao, Y. Liu, Y. Zhang, Y. Ye, W. Tress and C. Yi, *Sci. Adv.*, 2022, **8**, eabo7422.